Comput Geosci (2009) 13:469–481
DOI 10.1007/s10596-009-9138-x

ORIGINAL PAPER

Vertical equilibrium with sub-scale analytical methods for geological CO_2 sequestration

S. E. Gasda · J. M. Nordbotten · M. A. Celia

Received: 5 August 2008 / Accepted: 24 March 2009 / Published online: 23 April 2009

Abstract Large-scale implementation of geological CO_2 sequestration requires quantification of risk and leakage potential. One potentially important leakage pathway for the injected CO_2 involves existing oil and gas wells. Wells are particularly important in North America, where more than a century of drilling has created millions of oil and gas wells. Models of CO_2 injection and leakage will involve large uncertainties in parameters associated with wells, and therefore a probabilistic framework is required. These models must be able to capture both the large-scale CO_2 plume associated with the injection and the small-scale leakage problem associated with localized flow along wells. Within a typical simulation domain, many hundreds of wells may exist. One effective modeling strategy combines both numerical and analytical models with a specific set of simplifying assumptions to produce an efficient numerical–analytical hybrid model. The model solves a set of governing equations derived by vertical averaging with assumptions of a macroscopic sharp interface and vertical equilibrium. These equations are solved numerically on a relatively coarse grid, with an analytical model embedded to solve for wellbore flow occurring at the sub-gridblock scale. This vertical equilibrium with sub-scale analytical method (VESA) combines the flexibility of a numerical method, allowing for heterogeneous and geologically complex systems, with the efficiency and accuracy of an analytical method, thereby eliminating expensive grid refinement for sub-scale features. Through a series of benchmark problems, we show that VESA compares well with traditional numerical simulations and to a semi-analytical model which applies to appropriately simple systems. We believe that the VESA model provides the necessary accuracy and efficiency for applications of risk analysis in many CO_2 sequestration problems.

Keywords Geological CO_2 sequestration · Wellbore leakage · Vertical equilibrium method · Sharp interface models · Numerical simulation · Sub-scale analytical methods

1 Introduction

Recent reports by climate scientists have emphasized the high likelihood that global warming is occurring and will continue to accelerate unless action is taken to mitigate the projected doubling of CO_2 emissions over the next 50 years [1]. In order to make the necessary reduction in emissions in a timely manner, we must concentrate on scaling up technologies that are currently feasible from the pilot scale to the industrial scale [2]. One such immediately available technology is geological CO_2 sequestration that is associated with essentially zero-emission power plants. This strategy involves injecting the stream of CO_2, which would otherwise be

S. E. Gasda (✉)
Environmental Sciences and Engineering,
University of North Carolina at Chapel Hill,
Chapel Hill, NC, USA
e-mail: sgasda@unc.edu

J. M. Nordbotten
Department of Mathematics, University of Bergen,
Bergen, Norway

M. A. Celia
Civil and Environmental Engineering, Princeton University,
Princeton, NJ, USA

vented to the atmosphere, into permeable formations deep in the subsurface. This technology is promising because of extensive experience and infrastructure that already exist to facilitate the injection of fluids underground [3, 4]. However, the reliability and risk associated with injection operations needs to be examined and quantified to guide a proper regulatory framework required for CO_2 sequestration at massive scales.

A typical CO_2 injection operation in a deep saline aquifer involves supercritical CO_2 that is less dense and less viscous than the resident brine [5, 6]. The buoyant drive highlights the need for a competent caprock, and leads to concern about possible leakage through preferential pathways in the caprock [7, 8]. While saline aquifers have large storage capacity [9–12], their association with oil and gas operations, especially in North America, has resulted in many penetrations though caprock formations in the form of oil and gas wells [13, 14]. Because information about effective flow properties along old wells is very scarce [15], the parameters associated with leakage along wells will be relatively uncertain. As such, probabilistic analysis and Monte Carlo simulations are likely to be required. The appropriate model chosen in this framework needs to solve a complex system of many wells and multiple aquifers efficiently, without compromising accuracy.

The classic approach to modeling CO_2 injection employs fully three-dimensional numerical methods to solve the system with a high degree of accuracy [e.g., 16–19]. However, grid refinement is required wherever a potentially leaky well is present, and this leads to extreme computational demands involving many millions of grid cells. Therefore, for the problem of injection and potential leakage in domains that have three-dimensional layering and are characterized by many existing wells, traditional numerical simulators appear to be infeasible. In contrast to traditional simulators, under sufficiently simplifying assumptions much less computationally demanding models may be developed. Once such approach is to employ semi-analytical methods, which have been increasingly developed in recent years [6, 20–22]. Some of the key assumptions required to find an analytical solution are a homogeneous, horizontal aquifer, a sharp interface between the two fluids, and a radially symmetric injection plume. It should be noted that these assumptions are required for analytical solutions during the injection period, and can be relaxed during the post-injection period [see 23]. Within these constraints, the analytical methods are powerful tools and can be applied to complex leakage problems, including multiple realization Monte Carlo types of calculations [7, 8]. Yet another alternative is to solve the overall flow problem numerically but to embed a set of sub-scale analytical solutions for wellbore flow. Solving the system in this manner can speed up computation times substantially compared with traditional numerical methods, although it will never be as fast as an analytical method. However, the advantage of such a method is that complex geometry and heterogeneity in the large-scale system can be handled, which is not possible with an analytical method. This provides greater flexibility in the types of geological systems that can be modeled.

In this paper, we present a hybrid numerical–analytical approach to the computational challenges of modeling CO_2 injection. We will refer to this method as the Vertical Equilibrium with Sub-scale Analytical Model (VESA), because it combines a large-scale numerical model with embedded analytical solutions to capture sub-scale flow through leaky wells, constrained by the assumptions of a macroscopic sharp interface and vertical equilibrium in the pressure fields. In using VESA to model CO_2 injection, there are significant computational gains due to both the vertically averaged numerical method and the use of a local analytical solution. The end result is that the total number of grid cells is greatly reduced, while local behavior around leaky wells is still captured.

2 Methods

The VESA model presented herein employs a vertically averaged numerical model for large-scale flow coupled with an embedded analytical model for wellbore flow. The vertically averaged model is based on the assumption of vertical equilibrium, while the analytical model for wellbore flow is an extension of the classic upconing model that was presented by Nordbotten and Celia [24]. We will present a brief overview of both methods herein.

2.1 Vertically averaged flow in aquifers

Given the very strong density difference between the injected CO_2 and the resident brine [20], the system tends to exhibit very strong buoyant segregation [25]. An assumption of a macroscopic sharp interface is consistent with this behavior, and the underlying mathematics for such approximations is very well understood [26–30]. For self-consistency, we choose to give a brief review. To develop the equations to be solved in the numerical simulator, we begin with the three-dimensional system (x, y, z), where we have two fluids, the non-wetting (CO_2-rich) phase (n) and the wetting (brine) phase (w), separated by a sharp interface within

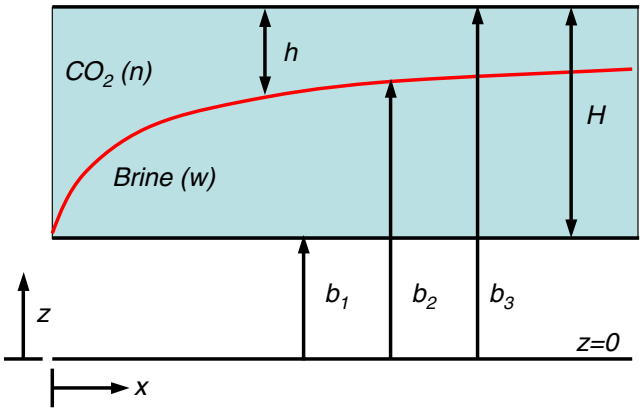

Fig. 1 Schematic of vertically averaged CO_2–brine system

an aquifer of thickness H (see Fig. 1). The system is initially saturated with the wetting phase. The distance from the datum at to the bottom of the aquifer is b_1, to the interface is b_2, and to the top of the aquifer is b_3. Thus, $b_3 - b_1 = H$ and $b_3 - b_2 = h$ as shown in Fig. 1. We consider incompressible flow within this system. For simplicity, we present the approximation for a primary drainage system, although the imbibition process is discussed later.

Starting with the basic balance equation for flow of each phase α in the system, where $\alpha = w, n$, we write,

$$\frac{\partial(\phi\rho_\alpha S_\alpha)}{\partial t} + \nabla\cdot\left(\rho_\alpha \mathbf{q}_\alpha\right) = \rho_\alpha F_\alpha. \tag{1}$$

In the above equation for phase α, where $\alpha = w$ or n, ϕ is the porosity, c_α is the fluid compressibility, ρ_α is the fluid density, S_α is the saturation, $\mathbf{q}_\alpha$ is the volumetric flux, and F_α is the source or sink term in units of volume per time. We take the vertical average of Eq. 1 for each phase α over the thickness of the respective phase, b_1 to b_2 for the brine phase, and b_2 to b_3 for the CO_2 phase. Given that saturation is constant in each region, the standard vertical averaging procedure [26–30] yields

$$\phi\rho_w\hat{\beta}_w (H-h)\frac{\partial p_w}{\partial t} + \phi\rho_w\left(1 - S^w_{\text{res}}\right)\frac{\partial}{\partial t}(H-h) + \nabla\cdot\rho_w\overline{\mathbf{q}}_w - \rho_w q_w|_{b_1} + \rho_w q_w|_{b_3} = \int_{b_1}^{b_2}\rho_w F_w dz, \tag{2a}$$

$$\phi\rho_n\hat{\beta}_n h\left(1 - S^w_{\text{res}}\right)\frac{\partial p_n}{\partial t} + \phi\rho_n\left(1 - S^w_{\text{res}}\right)\frac{\partial h}{\partial t} + \nabla\cdot\rho_n\overline{\mathbf{q}}_n + \rho_n\, q_n|_{b_3} - \rho_n\, q_n|_{b_1} = \int_{b_2}^{b_3}\rho_n F_n dz, \tag{2b}$$

where S^w_{res} refers to the residual wetting phase saturation, and the vertically averaged variables are denoted by an overbar with the volumetric fluxes having the following definitions,

$$\overline{\mathbf{q}}_w = \int_{b_1}^{b_2}\mathbf{q}_w dz, \tag{3a}$$

$$\overline{\mathbf{q}}_n = \int_{b_2}^{b_3}\mathbf{q}_n dz. \tag{3b}$$

Also in Eq. 2, $\hat{\beta}_\alpha$ refers to the vertically averaged compressibility of phase α, where β_α is a function of the fluid compressibility c_α and the matrix compressibility c_m such that $\beta_\alpha = c_m + \phi c_\alpha$. Note also in Eq. 2 that the height of the interface can be related to the vertically averaged phase saturations, $\overline{S}_w$ and $\overline{S}_n$ as,

$$\overline{S}_w = \frac{1}{H}\left[(H-h) + hS^w_{\text{res}}\right] \tag{4a}$$

$$\overline{S}_n = \frac{1}{H}\left[h\left(1 - S^w_{\text{res}}\right)\right] \tag{4b}$$

Under the assumption of vertical equilibrium, the vertical distribution of pressure p is fluid-static, such that,

$$p(x,y,z,t) = p_{\text{top}} + \begin{cases}\rho_n g(b_3 - z) & \text{for } b_2 < z < b_3\\ \rho_n g h + \rho_w g(b_2 - z) & \text{for } b_1 < z < b_2\end{cases}. \tag{5}$$

In the above expression, g is the acceleration due to gravity [L/T^2] and p_{top} refers to the pressure at the top of the aquifer, $p(x,y,t)|_{b_3}$. Use of Darcy's law then gives the following expressions for average horizontal fluxes in each phase,

$$\overline{\mathbf{q}}_w = -\frac{H\tilde{\mathbf{k}}_{r,w}\hat{\mathbf{K}}}{\mu_w}\left[\nabla p_{\text{top}} + \rho_w g\nabla b_3 - (\rho_w - \rho_n)g\nabla h\right], \tag{6a}$$

$$\overline{\mathbf{q}}_n = -\frac{H\tilde{\mathbf{k}}_{r,n}\hat{\mathbf{K}}}{\mu_n}\left[\nabla p_{\text{top}} + \rho_n g\nabla b_3\right], \tag{6b}$$

where μ_α is the viscosity [M (LT)$^{-1}$] of phase α, $\hat{\mathbf{K}}$ is the vertically averaged intrinsic permeability [L^2], where the average is taken from b_1 to b_3, and $\tilde{\mathbf{k}}_{r,\alpha}$ is the pseudo-relative permeability [L^0], obtained from the phase average over the thickness of phase α. This quantity is defined as:

$$\tilde{\mathbf{k}}_{r,w} = \frac{\hat{\mathbf{K}}^{-1}}{H}\int_{b_1}^{b_2}\mathbf{k}k_{r,w}dz, \qquad \tilde{\mathbf{k}}_{r,n} = \frac{\hat{\mathbf{K}}^{-1}}{H}\int_{b_2}^{b_3}\mathbf{k}k_{r,n}dz, \tag{7}$$

where $k_{r,\alpha}$ is the local relative permeability of phase α and $\mathbf{k}$ is the local value of intrinsic permeability [L^2].

More discussion of the pseudo-relative permeability will be provided in the next section.

We also observe that the two phase pressures differ by $p_n - p_w = -(\rho_w - \rho_n)(b_3 - h)g$, which looks like a type of capillary pressure because of the relationship between h and $\overline{S}_\alpha$ (although this derived capillary pressure is negative). This relationship in the vertically averaged system is often referred to as a pseudo-capillary pressure.

Together, Eqs. 2 and 6 form the system of equations that describes vertically averaged flow in an aquifer. The solution of these equations will give values for pressure in each phase $p_\alpha\,(x, y, z, t)$ and the thickness of CO_2 $h(x, y, t)$ in the two horizontal spatial dimensions and time.

2.1.1 Pseudo-relative permeability

The derivation presented above assumes that the system is undergoing primary drainage. This means that the system is initially fully saturated with brine, which is displaced by the injected CO_2, leaving only residual brine trapped behind the CO_2–brine interface. Because we have assumed a sharp interface between the two fluids, the local relative permeability within each phase, $k_{r,\alpha}$, is the endpoint value at maximum saturation of the phase, $k^\circ_{r,\alpha}$, as depicted in Fig. 2. In the case of the brine phase, the local relative permeability is $k^\circ_{r,w} = 1$ because the region is still fully saturated with the brine phase. For the CO_2 phase, the relative permeability

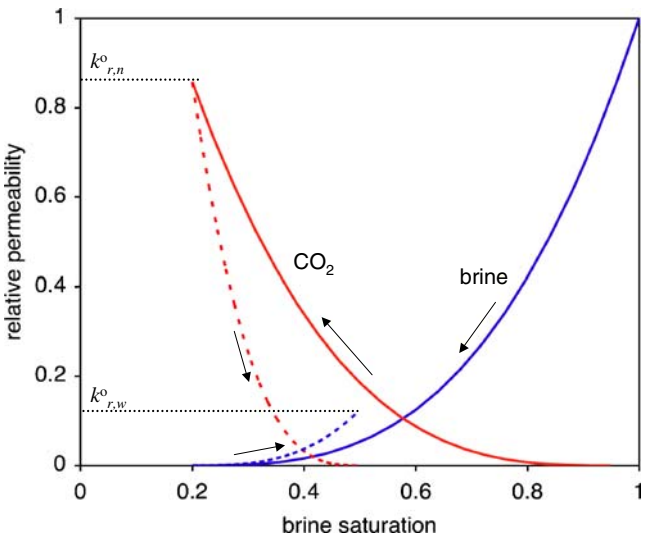

Fig. 2 Hypothetical local relative permeability drainage (*solid line*) and imbibition (*dotted line*) curves for CO_2 and brine. The maximum values of relative permeability for the CO_2 phase at residual brine and for the brine phase at residual CO_2 are indicated on the figure

at maximum saturation, $k^\circ_{r,n}$, is the value of the local function at $S_n = \left(1 - S^w_{\text{res}}\right)$. Within the context of a vertically averaged system, the local values of relative permeability are scaled by the height of the interface relative to the total thickness of the aquifer. The interface height can in turn be related to the vertically averaged saturation through Eqs. 4a and 4b, leading to *pseudo-relative permeability* functions. In the simple case where the intrinsic permeability is homogenous in the vertical direction, the pseudo-relative permeability functions reduce to scalars and are linear with respect to vertically averaged saturation.

$$\tilde{k}_{r,w} = \frac{H - h}{H} = \overline{S}_w - \frac{h}{H} S^w_{\text{res}}, \tag{8a}$$

$$\tilde{k}_{r,n} = k^\circ_{r,n} \frac{h}{H} = k^\circ_{r,n} \frac{\overline{S}_n}{\left(1 - S^w_{\text{res}}\right)}. \tag{8b}$$

Once the injection operation is completed, the system will undergo imbibition in some portions of the domain where the CO_2–brine interface is receding. The effect of residual entrapment on the longevity of CO_2 storage has been studied in recent works [23, 31]. It is still possible to have primary drainage along the leading edge of the plume, especially if there is angle to the top surface of the aquifer along which the CO_2 will migrate upslope over time. Residual CO_2 will be trapped in the pore space during imbibition, leaving some residual saturation of the CO_2 behind, up to 50% in some recent measurements [32]. This phenomenon leads to local and average relative permeability functions that are hysteretic in nature. Thus when solving this system, different relative permeability values are calculated depending on whether the system is in drainage or imbibition. It should be noted that residual CO_2 will only be trapped within the fraction of the aquifer between the current location of the interface and the historically lowest height of the interface at that spatial location, which corresponds to the maximum thickness of CO_2 which we refer to as $h_{\max}(x, y)$. Thus wherever imbibition has occurred, the vertically averaged phase saturations become,

$$\overline{S}_w = \frac{1}{H}\left[(H - h_{\max}) + h S^w_{\text{res}} + (h_{\max} - h)\left(1 - S^n_{\text{res}}\right)\right], \tag{9a}$$

$$\overline{S}_n = \frac{1}{H}\left[h\left(1 - S^w_{\text{res}}\right) + (h_{\max} - h)\, S^n_{\text{res}}\right]. \tag{9b}$$

The corresponding effective relative permeability functions are similar to those in the drainage case, except now instead of two regions with either fully saturated brine or partially saturated CO_2 with immobile brine, there is an additional region of partially saturated

brine with immobile CO_2. Therefore, the brine phase effective relative permeability needs to account for the additional region of partially saturated brine and the reduced local relative permeability in that region ($k^o_{r,w} < 1$),

$$\tilde{k}_{r,w} = \frac{1}{H}\left[H - h_{\max} + k^{\circ}_{r,w}\left(h_{\max} - h\right)\right]. \tag{10}$$

The relative permeability function for the CO_2 phase does not change during the imbibition process.

2.1.2 Numerical method

The vertically averaged equations described above are solved using a standard cell-centered finite-difference approximation. The system is solved using the IMPES method, first solving for pressure implicitly and then using an explicit calculation to determine the CO_2 thickness. The timestep used in the explicit solve is controlled by a CFL condition. The values of effective relative permeability in each cell are computed according to the equations described in Section 2.1.1. The upstream value of relative permeability is used at cell edges.

We have chosen to use the IMPES approach, but this system could be solved using an alternative numerical method. One aspect of the IMPES approach to note is that only the non-wetting phase equation is solved in the explicit saturation step. This leads to mass balance errors in the brine phase due to the system compressibility. However, the errors are small enough to have no significant effect on the solution. There are no mass balance errors for an incompressible system.

2.2 Analytical solution for wellbore flow

The embedded or local analytical solution used to solve for wellbore flow between two aquifers is taken from Nordbotten and Celia [24]. We refer to this solution as an upconing model because it extends early classic solutions that solve the problem of extracting a light fluid residing over a dense fluid using Dupuit-type assumptions [26, 28]. The solution to the upconing problem used herein uses a relaxed assumption for vertical equilibrium near the well. Specifically, non-zero vertical flow is allowed with the flow varying piecewise linearly in the z-direction with the maximum vertical flow occurring at the interface. The analytical solution is derived assuming an incompressible system, which is appropriate given that compressibility is more important at the large scale and not the local scale of a wellbore. Figure 3 shows a schematic of the underlying system in radial (r, z) coordinates. The well penetrates

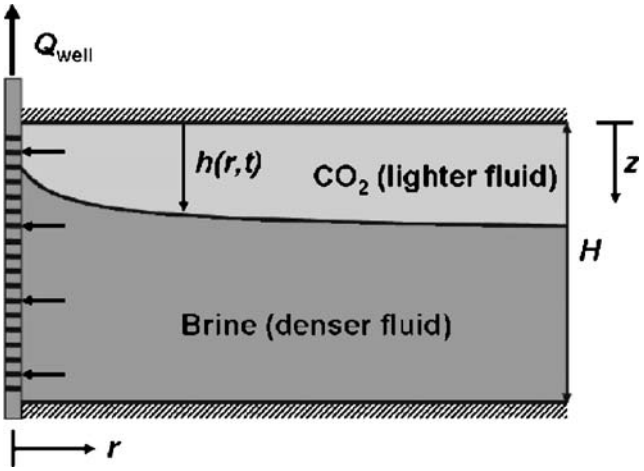

Fig. 3 Schematic of the CO_2–brine interface in the near-well region (obtained from [24])

the entire thickness of the aquifer and has a radius r_w and constant flow rate, Q_{well}. The solution for the interface is solved for all r, and if the thickness at $r = r_w$, $h(r_w, t)$ is greater than zero, then only the light fluid flows into the well. If the thickness is equal to zero, then both fluids can flow into the well.

To solve this system analytically, certain assumptions need to be made to simplify the system. In the original paper, three cases of different simplifying assumptions are analyzed. For the purposes of this work, we will implement the second case—a stationary interface, an outer boundary at a fixed distance, and flowing dense fluid. In this special case, a differential equation can be written, equation (29) in [24], and solved by satisfying the transcendental equation,

$$F\left(h', \eta\right) = F\left(h'_0, \eta_{\text{outer}}\right), \tag{11}$$

where h'_0 is the interface height at the outer boundary, and,

$$\begin{aligned} F\left(h', \eta\right) = {} & \frac{-1}{2\Gamma\lambda}\ln\left(\eta^2 - \frac{k'}{3\Gamma\lambda}\left(1 + (\lambda - 1)\,Q'_w\right)\right) \\ & - \frac{\left(h'\right)^2}{2\left(Q'_w\lambda + \left(1 - Q'_w\right)\right)} + \frac{h'\,Q'_w\lambda}{\left(Q'_w\lambda + \left(1 - Q'_w\right)\right)^2} \\ & + \frac{Q'_w\lambda(1 - Q'_w)}{\left(Q'_w\lambda + (1 - Q'_w)\right)^3} \\ & \times \ln\left(h'\,Q'_w\lambda - (1 - Q'_w)(h' - 1)\right). \end{aligned} \tag{12}$$

In Eqs. 11 and 12 above, Q'_w is the fractional flow of brine relative to the total volumetric flow rate, Q_{well},

such that $Q'_w + Q'_n = 1$. The following dimensionless quantities are employed,

$$\Gamma = \frac{2\pi\,(\rho_w - \rho_n)\,g k_r \lambda_w H^2}{Q_{\text{well}}},\; h' = \frac{h}{H},$$
$$\eta = \frac{r}{\sqrt{k_r}},\; k' = \frac{H^2}{k_z},\; \lambda = \frac{\lambda_n}{\lambda_w}. \tag{13}$$

In Eq. 13, λ_w and λ_n are the mobilities of the wetting and non-wetting phases, where mobility is defined as $k_{r,\alpha}/\mu_\alpha$, and k_r and k_z are the intrinsic permeability values in the radial and vertical directions, respectively.

It should be noted that the upper bound on Q'_w is given by the following limit as η_{outer} goes to infinity,

$$\lim_{\eta_{\text{outer}}\to\infty} Q'_w = \frac{1 - h'_0}{1 + h'_0\,(\lambda - 1)}. \tag{14}$$

Equation 14 defines the region in h–Q'_w space within which a solution to Eq. 11 exists.

The functional expression in Eq. 12 to describe upconing has a primary unknown quantity, Q'_w, which is the fractional flow of dense fluid into the well. The solution for Q'_w can be found given a value for h at the boundaries $\eta = \eta_{\text{inner}}$ and $\eta = \eta_{\text{outer}}$. We will discuss later how the values for h at the outer boundary and the location of the outer boundary, η_{outer}, are obtained. At the inner boundary, two-phase flow occurs when the value of h at η_{inner} equals 0, which is the point at which there are two phases in the well.

If the value of Q_{well} is prescribed, as it is for many applications of groundwater withdrawal or for some cases of oil and gas extraction, then solving Eqs. 11 and 12 is sufficient to determine the fractional flow of brine and CO_2 in the wellbore in an upconing scenario. However, in a leaky well system, the value of Q_{well} is unknown, and therefore additional equations must be written in order to close this system of equations. In this regard, we assume that wellbore leakage occurs predominantly along the exterior of the casing, through a zone that consists of well cement that may be degraded or poorly emplaced and the host rock that may be damaged to drilling action. Therefore, we can say that flow along the wellbore can be described by Darcy's law and an effective permeability, k_{well}, can be defined to describe the integrity of the wellbore at the bulk scale. The relative permeability function employed for wellbore flow is a linear function of phase saturation.

We use the following algorithm for the local upconing solution. First, the value of Q_{well} is determined by the flow of both phases in the wellbore,

$$Q_{\text{well}} = \pi r_w^2 \left(q^w_{\text{well}} + q^n_{\text{well}}\right), \tag{15}$$

where q^w_{well} and q^n_{well} are the volumetric fluxes of the brine and CO_2 phases, respectively, through the wellbore into the overlying aquifer. As discussed above, the flux of each phase α can be described by multiphase Darcy equations for flow in the vertical direction,

$$q^\alpha_{\text{well}} = -\frac{k_{\text{well}} k_{r,\alpha}\left(S^\alpha_{\text{well}}\right)}{\mu_\alpha}\left(\frac{p_{\text{well}} - p_{\text{top}}}{\Delta z_{\text{cap}}} - \rho_\alpha g\right), \tag{16}$$

where k_{well} is the bulk permeability of the wellbore, and the relative permeability $k_{r,\alpha}$ is the relative permeability as a function of the saturation of phase α in the wellbore, S^α_{well}. As described in Eq. 16, the pressure drive is approximated as a piecewise linear function across the thickness of the caprock, Δz_{cap}, where the difference in wellhead pressure is measured from the top of the lower aquifer (p_{well}) to the bottom of the upper aquifer (p_{top}). We also require that the two fluids fill the pore space in the wellbore,

$$S^w_{\text{well}} + S^n_{\text{well}} = 1. \tag{17}$$

In addition, we can relate the flux of the brine phase through the wellbore to the primary unknown of the upconing solution by means of Eqs. 15 and 16

$$Q'_w = \frac{\pi r^2 q^w_{\text{well}}}{Q_{\text{well}}}. \tag{18}$$

With the above set of equations describing wellbore flow, there are six equations, Eqs. 12, 15–18, and six primary unknowns Q'_w, Q_{well}, q^w_{well}, q^n_{well}, S^w_{well}, and S^n_{well}. Therefore, we have a closed set of equations, and a solution can be found for this system of equations given a set of boundary conditions. The details of obtaining boundary conditions from the global numerical solution are given in the following section.

2.3 Coupling in the VESA model

This section will give details of embedding the local analytical wellbore flow solution into the global numerical aquifer model. The general approach is to solve numerically the vertically averaged set of equations to determine flow and transport at the coarse scale. Then, the local problem is solved separately in any grid cell where there is a leaky well. At these spatial locations, the coarse-grid values for saturation and pressure are used as boundary conditions for the local upconing problem. The local upcoming problem is solved only once per global timestep.

2.3.1 Local–global coupling in vertically averaged equations

In the global solve on the coarse grid, the source/sink terms that appear in Eqs. 2a and 2b, $q_w|_{b_1}$, $q_w|_{b_3}$, $q_n|_{b_1}$, and $q_n|_{b_3}$, are set equal to the fluxes calculated in the local analytical solution. For general problems that involve slow, spatially extensive leakage across the caprock, these vertical flux terms would also include those leakage fluxes. Overall, these leakage terms account for all vertical fluxes across the caprock, and as such they represent the coupling to the local well-leakage and upconing solutions.

2.3.2 Defining boundary conditions for local upconing solution

One of the most important parts of the local upconing solution is the specification of boundary conditions. Assignment of boundary locations and values serve to couple the global solution to the local analytical upconing solution. We use the following algorithm. First, the coarse-grid saturation value for gridblock (i, j), $\overline{S}_n\big|_{i,j}$, can be used to approximate the boundary condition needed for the interface height h'_0 at the outer boundary in the local upconing solution. This assumption is reasonable when the spatial extent of upconing is much smaller than the size of the gridblock. We must also define the value of η_{outer} which is the location where the outer boundary condition is applied. In the analytical solution, the outer boundary is fixed at some arbitrary distance in order to solve for a stationary solution. In the numerical solution, we are solving for a steady-state local problem in a global solution that is transient. Because of this, we assume that the outer boundary is located at a distance that divides the global flow and the local flow into the well. This can be related to the familiar concept in groundwater hydrology known as the capture zone for a pumping well in uniform flow [27]. The capture zone defines the region around the well from which fluid enters the pumping well. Outside of this region, the flow bypasses the well. The width of this region, y, is related to the pumping well rate and the regional, or background, flux of fluid q_o and the height of the aquifer, H. The capture zone has a shape that encircles the well on the downstream side, and, on the upstream side, asymptotically approaches the lines,

$$y = \pm \frac{Q_{\text{well}}}{2 q_o H}. \tag{19}$$

Because we have a more complex flow system, involving two fluid phases and more complex upconing behaviors, we have generalized Eq. 19. The volumetric flux is summed over the phases, and we introduce two scaling parameters, c_r and β_r, and group terms so that some non-linear dependence can occur in the calculation of the outer boundary. The modified formula that we propose for the outer boundary location is as follows,

$$r_{\text{outer}} = c_r H \left(\frac{Q_{\text{well}}}{H^2 \sum_{\alpha} q_{o,\alpha}} \right)^{\beta_r}, \tag{20}$$

where $q_{o,\alpha}$ is the background flux of each phase α. This quantity is computed at each global timestep by taking an average over the phase fluxes through each of the four sides of the coarse gridblock in which the local upconing problem is solved. Recall that r_{outer} is related to η_{outer} by $\eta_{\text{outer}} = r_{\text{outer}}/\sqrt{K_r}$.

2.3.3 Wellhead pressure calculation

Now we turn to Eq. 16, where the values for pressure, p_{well} and p_{top}, are needed to calculate the wellbore fluxes. These values are not provided directly by the local upconing solution but instead must be obtained from the coarse-grid solution for pressure. To do this, we must first develop an equation that relates average pressure to local pressure when upconing is present. This relationship is based on the pressure correction originally presented by Peaceman [33], which relates average pressure to local pressure for a well flowing a single phase. The idea is to take a local expression for pressure variation in the vicinity of a well, for example a logarithmic function, and integrate it over the area of a grid cell to determine the associated cell-averaged pressure. For simple single-phase flow, the local pressure is defined by

$$p\,(r) = p_{\text{well}} + \frac{Q_{\text{well}}\mu}{2\pi k_{\text{well}} H} \left(\ln \frac{r}{r_w} \right). \tag{21}$$

Integration over the area of interest (from r_w to r_B) provides the following expression for average pressure, $\overline{p}$,

$$\overline{p} = p_{\text{well}} + \frac{Q_{\text{well}}\mu}{2\pi k_{\text{well}} H} \left(\ln \frac{r_B}{r_w} - \frac{1}{2} \right). \tag{22}$$

The value for r_B is usually obtained from a circle with equivalent area to the coarse gridblock of interest, $r_B = \sqrt{(\Delta x \Delta y)/\pi}$.

This same concept can be applied to the two-phase case by integrating over the pressure function, equation (13a) in [24], given an expression for the location of

the interface. For the interface, we consider a solution originally derived by Muskat [34] because it provides an explicit representation of the solution that cannot be obtained from the upconing solution presented in equation (28) in [24]. To arrive at Muskat's solution, we integrate the vertical-equilibrium form of equation (13a) in [24]. Muskat's approximation is obtained by further ignoring the effect of the variation of the interface on the pressure field, thus fixing $h(\eta, \tau) = h(\eta, 0)$ in equations (13d) and (13e) in [24]. Then, Muskat's solution (see [24, 34] for more details) can be written for two flowing phases as,

$$h' = h'_0 + \left(\frac{Q'_w}{\Gamma\left(1 - h'_0\right)} - \frac{1 - Q'_w}{\Gamma\lambda h'_0} \right) \ln \frac{\eta}{\eta_B}, \tag{23}$$

where the variables are defined as before. In general, we will consider

$$h' = h'_0 + F\left(Q'_w\right) \ln \frac{\eta}{\eta_B}, \tag{24}$$

where we define

$$F\left(Q'_w\right) = \frac{Q'_w}{\Gamma\left(1 - h'_0\right)} - \frac{1 - Q'_w}{\Gamma\lambda h'_0}. \tag{25}$$

To obtain the vertical-equilibrium form of the upconing pressure equation, equation (13a) in [24] is combined with Eqs. (13d) and (13e),

$$\frac{Q'_w}{\eta\Gamma\left(1 - h'\right)} = -\left(\frac{\partial p'}{\partial \eta} \right)\Big|_{z'=1}. \tag{26}$$

Equations 24 and 26 are combined to

$$\frac{\partial p'}{\partial \eta} = C_1 \frac{1}{\eta'\left(C_2 + \ln \eta'\right)}, \tag{27}$$

where,

$$C_1 = \frac{Q'_d}{\Gamma F\left(Q'_d\right)},\ C_2 = \frac{1 - h'_0}{F\left(Q'_d\right)},\ \text{and}\ \eta' = \frac{\eta}{\eta_B}. \tag{28}$$

Pressure as a function of the radial coordinate is obtained by integrating Eq. 27,

$$\begin{aligned} p'\left(\eta'\right) &= p'_B - \int_{\eta'}^{1} C_1 \frac{1}{\zeta\left(C_2 + \ln \zeta\right)} d\zeta \\ &= p'_B - C_1 \left[\ln C_2 - \ln\left(\ln\left(\eta' e^{C_2} \right) \right) \right] \end{aligned} \tag{29}$$

From Eq. 29, we obtain an expression for pressure at the wellhead, p_{well},

$$p'_{\text{well}} = p'_B - C_1 \left[\ln C_2 - \ln\left(\ln\left(\eta'_{\text{inner}} e^{C_2} \right) \right) \right], \tag{30}$$

where $\eta'_{\text{inner}} = \eta_{\text{inner}} / \eta_B$. The average pressure is obtained by integrating Eq. 29 over the area of interest,

$$\begin{aligned} \overline{p'} &= p'_B - C_1 \frac{\int_{\eta'_{\text{inner}}}^{1} \zeta \left[\ln C_2 - \ln\left(\ln\left(\zeta e^{C_2} \right) \right) \right] d\zeta}{\int_{\eta'_{\text{inner}}}^{1} \zeta d\zeta} \\ &= p'_B - C_1 \left[\ln C_2 - 2 \frac{\int_{\eta'_{\text{inner}}}^{1} \zeta \ln\left(\ln\left(\zeta e^{C_2} \right) \right) d\zeta}{1 - \left(\eta'_{\text{inner}} \right)^2} \right]. \end{aligned} \tag{31}$$

Finally, subtracting Eqs. 30 and 31, we obtain a relationship between the average pressure and the pressure at the wellhead,

$$\begin{aligned} &\overline{p'} - p'_{\text{well}} \\ &= -C_1 \left[\ln\left(\ln\left(\eta'_{\text{inner}} e^{C_2} \right) \right) - 2 \frac{\int_{\eta'_{\text{inner}}}^{1} \zeta \ln\left(\ln\left(\zeta e^{C_2} \right) \right) d\zeta}{1 - \left(\eta'_{\text{inner}} \right)^2} \right]. \end{aligned} \tag{32}$$

The integral in Eq. 32 must be evaluated numerically. Given this relationship, we can find the pressure at the wellhead that will be used in Eq. 16 for all values of Q'_w below the upper bound on Q'_w as defined in Eq. 14. As the coarse gridblock becomes 100% saturated with the light phase ($h'_0 = 1$ and $Q'_w = 0$), Eq. 32 reduces to the Peaceman expression for single-phase flow of the light fluid. For completeness, we also need an expression to relate the average pressure and local pressure in the upper aquifer. We choose to use the single-phase Peaceman expression from Eq. 22, which is a simplification of the actual pressure profile induced by two fluid phases flowing into the upper aquifer but seems reasonable if the flux of the light phase is small.

Now we have a complete set of equations and boundary conditions to solve the local upconing problem. We follow an algorithm where, first, the gridblock pressures are used to find the local wellhead pressures used in Eq. 32. Then, the non-linear system of upconing equations is solved using the secant method.

3 Model application

In this section, we present results obtained from applying the VESA model to several CO_2 injection problems. The first set of problems involves two of the three benchmarks proposed by the 3rd Annual CO_2 Modeling Workshop in Stuttgart, Germany [35]. These benchmarks were used to compare 12 different models developed at institutions in the US and Europe, and thus provide a useful verification of the VESA model. The second set of problems is an expanded version of the third benchmark where CO_2 injection and migration is modeled within the Johansen Formation, a prospective saline formation off the Norwegian coast in the North Sea. In this modified version of Benchmark 3, the entire formation is modeled using data covering areal extent of over 2,100 km^2, more than 100 times larger than the original benchmark problem.

3.1 Stuttgart benchmark problems

The VESA model presented herein was applied to benchmark problems used in the model comparison study described in [35]. The first benchmark (1.1) is a modified version of a two-aquifer system with a single leaky well presented originally in Nordbotten et al. [21]. The second set of benchmarks (problems 3.1 and 3.2) model long-term CO_2 injection and migration within the Johansen Formation. This benchmark uses different relative permeability functions, either with or without hysteresis in the imbibition phase, for problems 3.1 and 3.2, respectively.

For complete descriptions of the benchmark problems as well as results from all of the models, including VESA, the reader is referred to [35]. Herein we comment on the results but do not reproduce them. We see from the results for Benchmark 1.1 that the VESA model compares well with other models in the comparison study. The magnitude and timing of the peak leak rate match well with the other models, ranging from the Princeton semi-analytical method (Elsa) to sophisticated numerical models like ECLIPSE (Schlumberger, Paris), which produces results essentially identical to VESA in both the peak leak rate and long-term decline of the leakage rate.

In regard to Benchmarks 3.1 and 3.2, the comparison is more difficult because the other models used to solve this problem all employ traditional, 3D numerical methods and the test problem requested from each modeling group a contour plot of CO_2 saturation at the top surface indicating saturations of 0.2, 0.5, and 0.8. However, due to the assumptions of a sharp interface and complete segregation of the fluids by gravity in the VESA model, the CO_2 saturation at the top surface is equal to maximum saturation at residual brine, $S_n = \left(1 - S^w_{\text{res}}\right)$, at every location within the areal extent of the CO_2 plume. Therefore, we chose to submit results indicating the location of the plume outer edge for comparison with the other models.

The main observation about the comparison of VESA with other models is that the simplified vertical-equilibrium model compares well with more complex and sophisticated codes such as MUFTE-UG and ECLIPSE for problems with small-scale wellbore flow and complex geological systems. We are confident in the ability of this method to handle leaky wells using accurate and efficient sub-scale analytical solutions, as we see from comparison in Benchmark 1. The good comparison in Benchmark 3 shows that VESA can model complex geometry and heterogeneity of actual geological formations. Thus, we can conclude that a simplified method, such as VESA, can capture the essential physics of these systems using many fewer grid nodes than a traditional 3D method.

One key aspect to the VESA model is the increase in computational efficiency for both types of problems. The greatest computational gains occur in the Benchmark 1.1, where VESA can perform calculations in minutes versus hours for the other models in the comparison study. The computational gains are due to the reduction in the number of unknowns by reducing the z-dimension and the local grid refinement around the leaky well. The amount of gridblocks used by VESA for the wellbore problem was 1,026 nodes, compared with 60,000 to over 4,000,000 for the other models in the study. For Benchmark 3.1, the gains in efficiency are not as marked, and VESA performs faster than a most models but slower than four models that participated in this benchmark. We would expect to perform faster than all of the models in the study due to the reduction in the number of unknowns by factors between 5 and 10. This is likely due to the solver and other compilation aspects of VESA that are not optimized for computational efficiency. These issues need to be resolved in the future before a direct comparison can be made with more sophisticated models.

3.2 Johansen Formation

In addition to the benchmark problems, the VESA model was applied to the full Johansen Formation, using the dataset from which a subset was taken for Benchmark 3. The domain for the full Johansen Formation is almost two orders of magnitude larger than the domain for the benchmark problem. The Johansen Formation is described in more detail in [35] and [36],

and therefore only a brief description will be provided herein.

3.2.1 System description

The portion of the Johansen Formation used in this problem spans an areal extent over 2,100 km^2. The formation geometry is shown in Fig. 4. The defining feature is a fault that splits the back half of the formation into a shallower and a deeper portion. The fault is considered to be closed and does not provide hydraulic communication between the shallow and deep sections. The depth of the top of the formation ranges from 2,000 to 3,300 m below the surface. Formation thickness varies from 30 m to 225 m with an average thickness of 111 m, with a spatial distribution shown as grayscale contours in Fig. 4. The porosity and permeability data were vertically averaged as required by the VESA model, and the areal distributions of each parameter are shown in Figs. 5 and 6. We can see from Fig. 5 that the porosity generally varies from 10% in the lower left to 27% in the upper right corner, increasing with decreasing depth. Permeability varies from 570 mDarcy (1 mDarcy $= 10^{-15}$ m^2) to 0.01 mDarcy and generally increases with decreasing depth, but with a more complicated distribution. There is an abrupt change in permeability along a diagonal from the lower right corner to the beginning of the fault.

The formation is modeled as a confined aquifer, with fixed pressure boundaries along the outer edge corresponding to a hydrostatic pressure condition. There are no-flow boundary conditions at the top and bottom of the formation. The density of CO_2 is 479 kg/m^3 and the density of brine is 1,045 kg/m^3, which are the reference values at 30 MPa, while the viscosity values are 0.0395 and 0.2535 mPa s for the CO_2 and brine, respectively. These fluid properties correspond to a deep and relatively warm aquifer. The fluids and the porous matrix are considered to be compressible, with the compressibility factor c_α equal to 4.6×10^{-10} Pa^{-1} for the brine and 7.25×10^{-9} Pa^{-1} for CO_2. The formation compressibility is 1.0×10^{-10} Pa^{-1} which is a typical value for a consolidated sandstone. The spatial discretization is a relatively coarse mesh composed of 8,418 equal-sized cells, each with dimensions of 500 × 500 m.

CO_2 is injected into a system initially saturated with brine. Two injection scenarios are modeled. The first is a single well located at $x = 32.25$ km and $y = 29.75$ km injecting at a constant rate of 30 kg/s, which is twice the injection rate of the original benchmark problem. The second scenario consists of four wells injecting 15 kg/s each, with the wells located on the

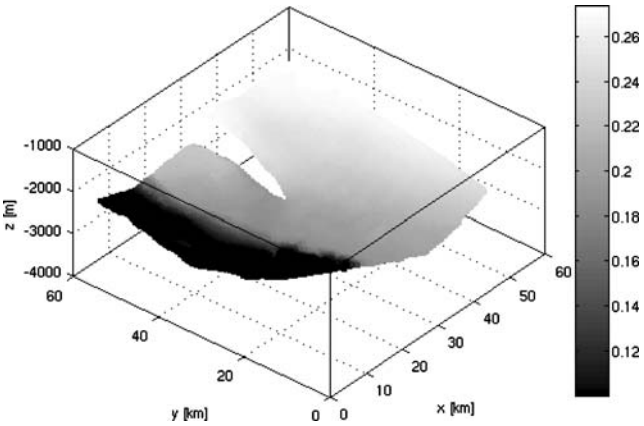

Fig. 5 Spatial distribution of vertically averaged porosity within the Johansen Formation

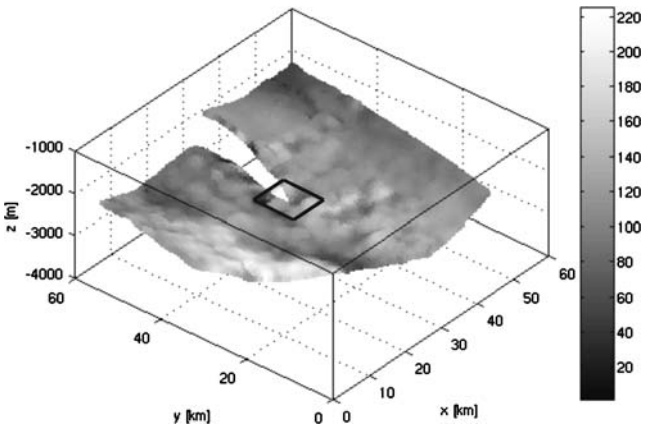

Fig. 4 Geometry of the Johansen Formation showing the spatial distribution of thickness in meters. The small outlined region in the center portion of the figure delineates the domain of the Johansen formation used in Benchmark 3

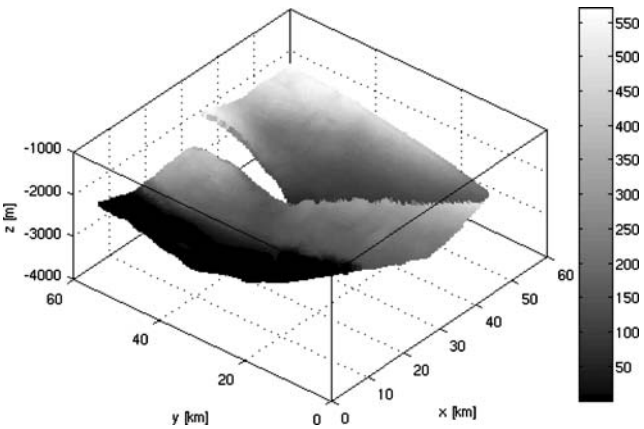

Fig. 6 Spatial distribution of vertically averaged permeability [mDarcy] within the Johansen Formation

corners of a square having dimension equal to 2,500 m. The (x, y) locations of the four wells are: (32.25 km, 29.75 km), (32.25 km, 32.25 km), (34.75 km, 29.75 km), and (34.75 km, 32.25 km). In each of the two scenarios, the total simulation time is 100 years with CO_2 injection occurring at a constant rate for the first 50 years, with natural plume migration allowed to occur for the second 50 years.

For this test problem, the residual saturation values are set to 0.20 and 0.50 for the brine and CO_2 phases, respectively. These values are the same as used in Benchmark 3 discussed above. The endpoint value at maximum saturation needed for the pseudo-relative permeability functions (as discussed in Section 2.1.1) assumes local relative permeability functions to be simple cubic functions. This results in $k^{\circ}_{r,n}$ equal to 0.512 for the CO_2 phase and $k^{\circ}_{r,w}$ equal to 0.125 for the brine phase (in regions of residual CO_2 created by imbibition).

3.2.2 Simulation results

The results are plotted as a single contour indicating the outer edge of the CO_2 plume after 2, 50, and 100 years for both injection scenarios, a single well in Fig. 7 and four wells in Fig. 8. The depth of the formation top is also shown in the background of the contour plot for reference. In the single well case, the plume has extended approximately 10 km in the x-direction and 7 km in the y-direction after 50 years. The plume is skewed updip towards the right-hand side of the figure.

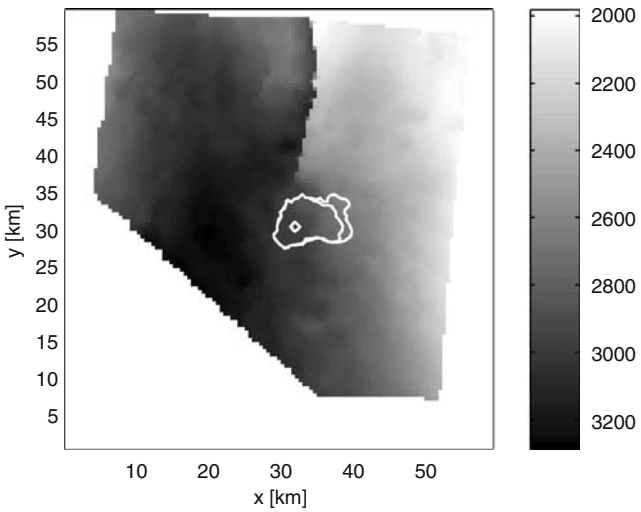

Fig. 7 Contours indicating the outer edge of the CO_2 plume at 2 years, 50 years and 100 years for a single well injecting 30 kg/s for the first 50 years. The background grayscale indicates depth of the formation top in meters

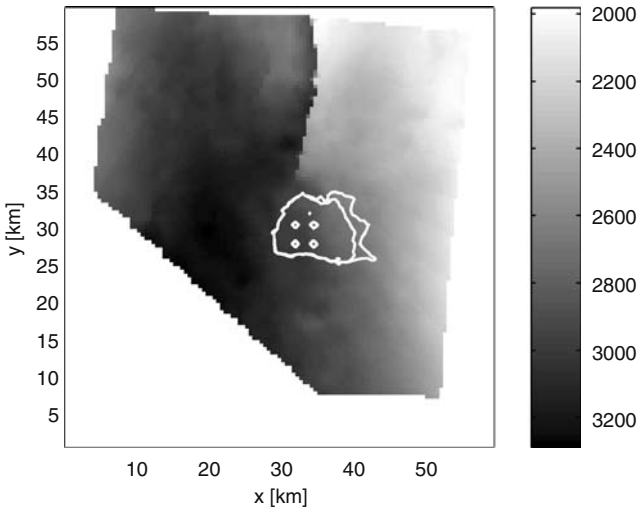

Fig. 8 Contours indicating the outer edge of the CO_2 plume at 2, 50, and 100 years for four wells injecting a total of 60 kg/s for the first 50 years. The background grayscale indicates depth of the formation top in meters

Once injection has ceased, the plume continues its updip migration, expanding at the upslope edge by a kilometer. As the back of the plume migrates upslope a large amount of residual CO_2 is entrapped in the pore space. In Fig. 7, the residual CO_2 appears to be part of the plume, but the residual phase is immobile. After 100 years, approximately 25 million tons of CO_2 is trapped in the residual phase, accounting for 55% of the total amount injected.

For the multi-injector case, the plume extends nearly 12 km in the x-direction and around 9 km in the y-direction. As in the single injector case, the plume is shifted noticeably updip, expanding upslope by 3 km, while residual CO_2 is left entrapped behind the retreating downslope edge of the plume. One significant difference in the four-well case is that the 100-year plume shape has three fingers in the upslope edge that have lengths of about 2 km and are nearly 1 km wide. At 100 years, 47 million tons of CO_2 have been trapped in the pore space, equaling 50% of the injected mass.

The computational effort for both injection scenarios was equal, taking just under 3 h to solve for pressure and interface height on 8,418 nodes over a 100-year simulated period.

One final aspect of the Johansen Formation results is the evolution of pressure during and after injection. It is important to examine the pressure at the injection well in order to ensure that fracture pressures are not exceeded in the reservoir. There are several factors that affect near-well pressure, including the injection rate, permeability and thickness of the formation, the confinement along the top and bottom boundaries, and

the treatment of the outer boundary condition. In this study, the caprock is assumed to be impermeable to flow by both the CO_2 and brine phases, and fixed pressure conditions are imposed at the outer boundary. The combination of these boundary conditions causes an initial sharp increase in the pressure at the injection well, followed by a slow decrease in pressure over time, similar to results shown in [36]. This evolution is typical of a fixed pressure outer boundary condition, where pressure does not build up in the domain because flow is allowed to occur out of the system along the outer boundary. The effect of zero flux top and bottom boundary condition accounts for the rate of pressure decline at the injection well. If brine were allowed to flow in a diffuse manner through the caprock, pressure would propagate through the caprock and cause a lower overall pressure buildup near the injection well. However, in this case, there would be increased pressure in layers farther up in the geological sequence.

4 Conclusion

A novel method for modeling geological CO_2 sequestration has been presented in this paper. The VESA model combines a vertical-equilibrium numerical method with sub-scale analytical solutions, and can model both large-scale flow in aquifers and small-scale flow through leaky wells. Assumptions of vertical equilibrium and a sharp interface allow us to reduce a large 3D flow problem to a more tractable 2D problem. The 2D vertical-equilibrium problem is then discretized in horizontal space and solved numerically with a standard finite-difference method, giving the necessary flexibility to handle complex formation geometry and large-scale heterogeneity. The VESA model has the ability to capture sub-scale wellbore flow by employing an analytical interface solution and Peaceman-like pressure correction instead of using traditional grid refinement. The combination of vertical averaging and sub-scale analytical method allows for significant increases in computational efficiency.

The VESA model was tested in a series of benchmark problems in order to compare results with a number of different simulators. The first application was a simplified two-aquifer system connected by flow through a single leaky wellbore. The second problem used a subset of geologic data from the Johansen Formation in the North Sea to provide a heterogeneous and geologically complex system for modeling CO_2 injection and migration both before and after injection is shut off. The third application expanded the latter problem to include the entire dataset for the Johansen Formation, significantly increasing the lateral extent of the domain. In this problem, the use of a single and multiple injection wells was investigated over longer injection and shut-off periods.

The results from the VESA model were compared with a variety of models from different institutions. These models vary in sophistication of the numerical scheme and complexity of the physical, chemical, and thermal processes included; however, the commonality is that all model the full three-dimensional problem. Upon comparison, we conclude that the VESA model, despite its simplicity, compares well with sophisticated 3D simulators in terms of the evolution of wellbore flow tested in the first problem or in terms of the location of the CO_2 plume after 25 or 50 years in the second problem. In addition, the VESA model achieves similar results but with significantly faster computational times in some cases. We estimate for the first simplified system including wellbore flow, the VESA model ranges from 100 to 100,000 times faster than other simulators. For more general formations and larger domain sizes, the increase in efficiency is less significant, with some simulators performing better than the VESA model by a factor of 2 or more. It is clear from this comparison that the VESA model has much room for computational improvements, especially because we have not yet attempted any significant algorithmic optimization. This, as well as the parallelization of the model, is the subject of ongoing work.

This study demonstrates that there is a viable alternative to traditional numerical methods that can capture the essential large- and small-scale features of geological CO_2 sequestration but at significantly lower computational cost. Although traditional methods will remain useful for a variety of applications, including detailed study of complex physical, chemical, and thermal processes, their utility is often limited to systems where detailed data is readily available and they can be limited by excessive computational demands, especially for problems involving multiple leaky wells. The VESA model presented herein, on the other hand, provides computational efficiency at the expense of some of the broader physics and chemistry involved in the problem. However, for many systems and applications, these assumptions are reasonable, and the resulting computational results represent the system well. The test problem results associated with the current study demonstrate this clearly, thereby giving us confidence that the VESA model captures much of the essential physics of the problem.

Acknowledgements This work was funded in part by a grant to from BP through funding of the Carbon Mitigation Initiative

at Princeton University, and the King Abdullah University of Science and Technology through a research fellowship for S. Gasda (Award no. KUS-F1-026-41).

References

1. Intergovernmental Panel on Climate Change (IPCC): Climate change 2007: the physical science basis. Fourth assessment report, IPCC Secretariat, Geneva, Switzerland (2007)
2. Socolow, R.H.: Can we bury global warming? Sci. Am. **293** (1), 49–55 (2005)
3. Pacala, S., Socolow, R.: Stabilization wedges: solving the climate problem for the next 50 years with current technology. Sci. **305**, 968–972 (2004). doi:10.1126/science.1100103
4. Bachu, S.: CO_2 storage in geological media: role, means, status and barriers to deployment. Prog. Energy Combust. Sci. **3**(2), 254–273 (2008). doi:10.1016/j.pecs.2007.10.001
5. Bachu, S.: Sequestration of CO_2 in geological media in response to climate change: road map for site selection using the transform of the geological space into the CO_2 phase space. Energy Convers. Manag. **43**(1), 87–102 (2003). doi:10.1016/S0196-8904(01)00009-7
6. Nordbotten, J.M., Celia, M.A., Bachu, S.: Analytical solutions for leakage rates through abandoned wells. Water Resour. Res. **40**(4), W04204 (2004). doi:10.1029/2003WR002997
7. Celia, M.A., Bachu, S., Nordbotten, J.M., Kavetski, D., Gasda, S.E.: A risk assessment tool to quantify CO_2 leakage through wells in mature sedimentary basins. 8th International Greenhouse Gas Control Technologies (2006)
8. Bachu, S., Celia, M.A.: Assessing the potential for CO_2 leakage, particularly through wells, from geological storage sites. In: McPherson, B.J.O.L., Sundquis, E. (eds.) The Science of CO_2 Storage, AGU monograph, in press. American Geophysical Union, Washington, DC (2009)
9. Koide, H.G., Tazaki, Y., Noguchi, Y., Nakayama, S., Iijima, M., Ito, K., Shindo, Y.: Subterranean containment and long-term storage of carbon dioxide in unused aquifers and in depleted natural gas reservoirs. Energy Convers. Manag. **33**(5–8), 619–626 (1992). doi:10.1016/0196-8904(92)90064-4
10. Holloway, S.: Storage of fossil fuels-derived carbon dioxide beneath the surface of the earth. Annu. Rev. Energy Environ. **26**, 145–166 (2001). doi:10.1146/annurev.energy.26.1.145
11. Bruant, R.G., Guswa, A.J., Celia, M.A., Peters, C.A.: Safe storage of CO_2 in deep saline aquifers. Environ. Sci. Technol. **36**(17), 240A–245A (2002). doi:10.1021/es0223325
12. Intergovernmental Panel on Climate Change (IPCC): Special report on carbon dioxide capture and storage. Cambridge University Press, Cambridge (2005)
13. Energy Information Administration (EIA): Annual Energy Review 2005, DOE/EIA-0384 (2005)
14. Gasda, S.E., Bachu, S., Celia, M.A.: Spatial characterization of the location of potentially leaky wells penetrating a deep saline aquifer in a mature sedimentary basin. Environ. Geol. **46**, 707–720 (2004). doi:10.1007/s00254-004-1073-5
15. Gasda, S.E., Nordbotten, J.M., Celia, M.A.: Determining effective wellbore permeability from a field pressure test: a numerical analysis of detection limits. Environ. Geol. **54**(6), 1207–1215 (2007). doi:10.1007/s00254-007-0903-7
16. White, M.D., Oostrom, M.: STOMP, Subsurface Transport Over Multiple Phases. Pacific Northwest National Laboratory, Report PNNL-11218, Richland, WA (1997)
17. Pruess, K., Oldenburg, C., Moridis, G.: TOUGH2 User's Guide, Version 2.0, Lawrence Berkeley National Laboratory Report LBNL-43134. Berkeley, CA (1999)
18. Pruess, K., García, J., Kovscek, T., Oldenburg, C., Rutqvist, J., Steefel, C., Xu, T.: Code intercomparison builds confidence in numerical simulation models for geologic disposal of CO_2. Energy **29**(9–10), 1431–1444 (2004). doi:10.1016/j.energy.2004.03.077
19. Schlumberger: Eclipse Technical Description 2007.1 (2007)
20. Nordbotten, J.M., Celia, M.A., Bachu, S.: Injection and storage of CO_2 in deep saline aquifers: analytical solution for CO_2 plume evolution during injection. Transp. Porous Media **58**(3), 339–360 (2005). doi:10.1007/s11242-004-0670-9
21. Nordbotten, J.M., Celia, M.A., Bachu, S.: Semianalytical solution for CO_2 leakage through an abandoned well. Environ. Sci. Technol. **39**(2), 602–611 (2005). doi:10.1021/es035338i
22. Nordbotten, J.M., Kavetski, D., Celia, M.A., Bachu, S.: A semi-analytical model estimating leakage associated with CO_2 storage in large-scale multi-layered geological systems with multiple leaky wells. Environ. Sci. Technol. **43**(3), 743–749 (2009)
23. Hesse, M.A., Orr, F.M., Jr., Tchelepi, H.A.: Gravity currents with residual trapping. J. Fluid Mech. **611**, 35–60 (2008). doi:10.1017/S002211200800219X
24. Nordbotten, J.M., Celia, M.A.: An improved analytical solution for interface upconing around a well. Water Resour. Res. **46**(8), W08433 (2006). doi:10.1029/2005WR004738
25. Nordbotten, J.M., Celia, M.A.: Similarity solutions for fluids injected into confined aquifers. J. Fluid Mech. **561**, 307–327 (2006). doi:10.1017/S0022112006000802
26. Bear, J.: Dynamics of Fluids in Porous Media. Elsevier, New York (1972)
27. Bear, J.: Hydraulics of Groundwater. McGraw-Hill, New York (1979)
28. Lake, L.: Enhanced Oil Recovery. Prentice Hall, Upper Saddle River (1989)
29. Coats, K.H., Dempsey, J.R., Henderson, J.H.: The use of vertical equilibrium in two-dimensional simulation of three-dimensional reservoir performance. Soc. Pet. Eng. J. **11**(1), 63–71 (1971). doi:10.2118/2797-PA
30. Dietz, D.N.: A theoretical approach to the problem of encroaching and by-passing edge water. In: Proceedings Akademie van Wetenschappen, pp. 83–94 (1953)
31. Juanes, R., Spiteri, E.J., Orr, F.M., Jr., Blunt, M.J.: Impact of relative permeability hysteresis on geological CO_2 storage. Water Resour. Res. **42**, W12418 (2006). doi:10.1029/2005WR004806
32. Bachu, S., Bennion, B.: Effects of in-situ conditions on relative permeability characteristics of CO_2–brine systems. Environ. Geol. **54**, 1707–1722 (2008). doi:10.1007/s00254-007-0946-9
33. Peaceman, D.W.: Interpretation of wellblock pressures in numerical reservoir simulation. Soc. Pet. Eng. J. **6**, 183–194 (1978)
34. Muskat, M.: Physical Principles of Oil Production. McGraw-Hill, New York (1949)
35. Class, H., Ebigbo, A., Helmig, R., Dahle, H., Nordbotten, J.M., Celia, M.A., Audigane, P., Darcis, M., Ennis-King, J., Fan, Y., Flemisch, B., Gasda, S., Krug, S., Labregere, D., Min, J., Sbai, A., Thomas, S., Trenty, L.: A benchmark study on problems related to CO_2 storage in geologic formations. Comput. Geosci. (2009; this issue)
36. Eigestad, G.T., Dahle, H.K., Hellevang, B., Johansen, W.T., Riis, F., Øian, E.: Geological Modeling and Simulation of CO_2 injection in the Johansen Formation. Comput. Geosci. (2009; this issue)